IPTC-22425-MS

Experimental and Numerical Analysis of Thermal EOR Recovery Schemes for Extra-Heavy Oil of the Oykino-Altuninsky Uplift of the Romashkinskoye Oilfield

Anastasia Pituganova, Kazan Federal University; Taofik Nassan and Mohd Amro, Technical University Bergakademie Freiberg; Ilgiz Minkhanov, Mikhail Varfolomeev, and Alexander Bolotov, Kazan Federal University

 DOI 10.2523/IPTC-22425-MS

This paper was prepared for presentation at the International Petroleum Technology Conference held in Riyadh, Saudi Arabia, 21-23 February 2022.

Abstract

Crude oil production from conventional oil reservoirs is declining owing to heavy exploitation to meet the global energy market demand which is growing on a yearly basis. Unconventional oil resources, e.g. extra-heavy oil and bitumen, can compensate for this decline if appropriate enhanced oil recovery (EOR) methods are developed to enable economic flow from these resources. The main objective of this study is to set the best practice for the extra-heavy oil production of the Oykino-Altuninsky uplift of the Romashkinskoye oilfield (Tatarstan Republic, Russia). A series of experimental tests are applied on a real unextracted unconsolidated core sample from Romashkinskoye oilfield where the viscosity of the crude oil is above 600,000 cP at reservoir conditions. Different recovery schemes are tested experimentally and sequentially, namely: water flooding, hot water flooding, steam flooding, and finally in-situ combustion (ISC). Furthermore, the complete experimental run is simulated by a standard nonisothermal simulator and the results are compared to the experiments. On contrary to what was expected hot water at 100°C didn't achieve any recovery from the sample and steam injection recovered only 11,5% of OOIP. ISC-is also known as fire flooding-attained the best recovery which reached 45% after steam flooding. Complete SARA analysis of the original oil and produced oil by steam and ISC is implemented to understand the mechanisms of each process. Numerical modeling is applied to the corresponding laboratory experiments and the results for water, hot water, and steam flooding were in good agreement with the experimental results while the in-situ combustion simulation showed a better recovery factor than experiments. The laboratory and numerical experiments will improve our understanding of the recovery options of Oykino-Altuninsky uplift of the Romashkinskoye oilfield and help the developers to choose the best production sequence for this oilfield particularly. Moreover, the experiments will provide inputs for the field-size numerical model after running more experiments on unconsolidated and consolidated cores.

Introduction

The development of enhanced oil recovery (EOR) techniques has been ongoing since the second half of the last century. The driving force to develop EOR techniques is the decline in the production of the existing producing reservoirs where the operators realized that a significant amount of oil (about 60-70%) remained in their reservoirs after primary and secondary recovery. This situation is even worse in heavy oil reservoirs. Figure 1 illustrates the approximate production share of EOR methods according to crude classification.

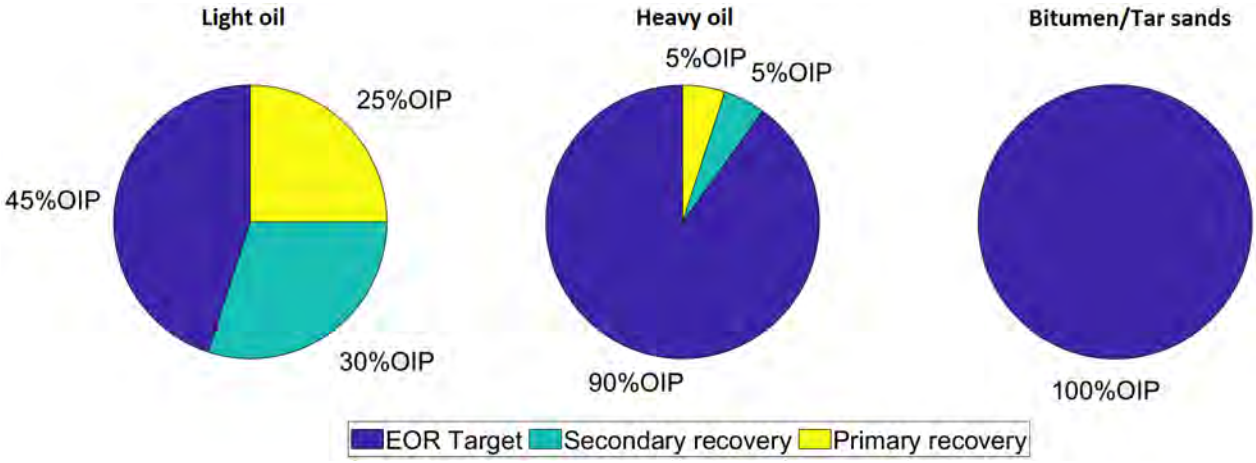

Figure 1—EOR production share from original oil in place (OIP) for different oil types (Lake, 2010; Green and Willhite, 2018).

Heavy oils are characterized by low API gravity and high viscosity (>100cP), as shown in Table 1 (Lake et al., 2014). Heavy oil reserves account for about 70% of the total proved oil reserves (Figure 2). Heavy oil will dominate energy markets in the future owing to the abundant reserves worldwide and the depletion of conventional light oil resources.

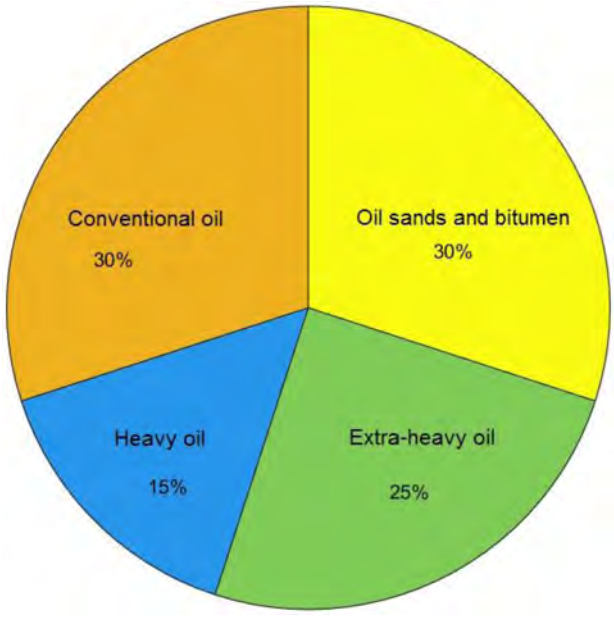

Figure 2—Total world oil reserves according to API classification (Alboudwarej et al., 2006).

Table 1—Crude oil classification (Lake et al., 2014)

Crude type	°API	Viscosity, cP	Remarks
Light and medium/Conventional oil	>22	<100	
Heavy oil	<22	>100	
Extra-Heavy crude	<10	>10,000	
Natural bitumen	<10	>1000,000	also called Tar or Oil sands

Due to the high viscosity, the development of heavy oil reservoirs is more difficult in comparison to the conventional oils. The traditional methods like water injection or gas injection are less effective for extracting the heavy oil. In some cases, if the oil viscosity is not so high (maximum up to 10,000 cp), cold water injection can be used for the production of heavy oils, followed by thermal EOR (Arcelus-Arrillaga et al., 2017; Nassan and Amro, 2021). For many reservoirs, thermal methods should be used in the initial stage of reservoir development as water injection is ineffective. Currently, steam injection is actively used in Latin America, USA, Canada, China, and Russia. However, during the application of steam injection, it has showed more and more problems including (Hamedi et al., 2013; Yi et al., 2018; Al-Muntaser et al., 2019):

1. A large volume of water is required (high steam to oil ratio (SOR));
2. High cost and environmental problems caused by burning a large amount of coal or natural gas to produce steam, huge fresh water consumption, and a large amount of produced water (water treatment issues);
3. Limitation of viscosity reduction.

Also, for heavy oils, operators are facing another problem that is the difficulties in the transportation to oil refinery (Al-Murayri et al., 2016).

All these practical issues and problems can be eased by an in-situ oil upgrading process using in-situ combustion (ISC), which eliminates the need for water, improves sweep efficiency, and finally upgrades the oil and make it pumpable. A review of the most important ISC projects in the world leads to the results illustrated in figures 3 and 4 (Koottungal, 2014). It can be seen from both figures the broad range of application of this method for different oils and depths.

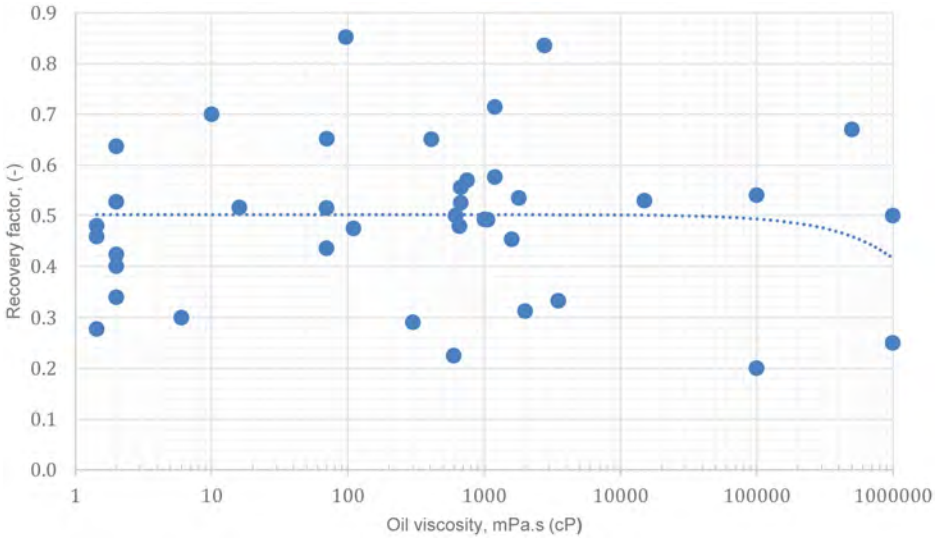

Figure 3—Recovery factor vs. viscosity for ISC projects around the world (Koottungal, 2014).

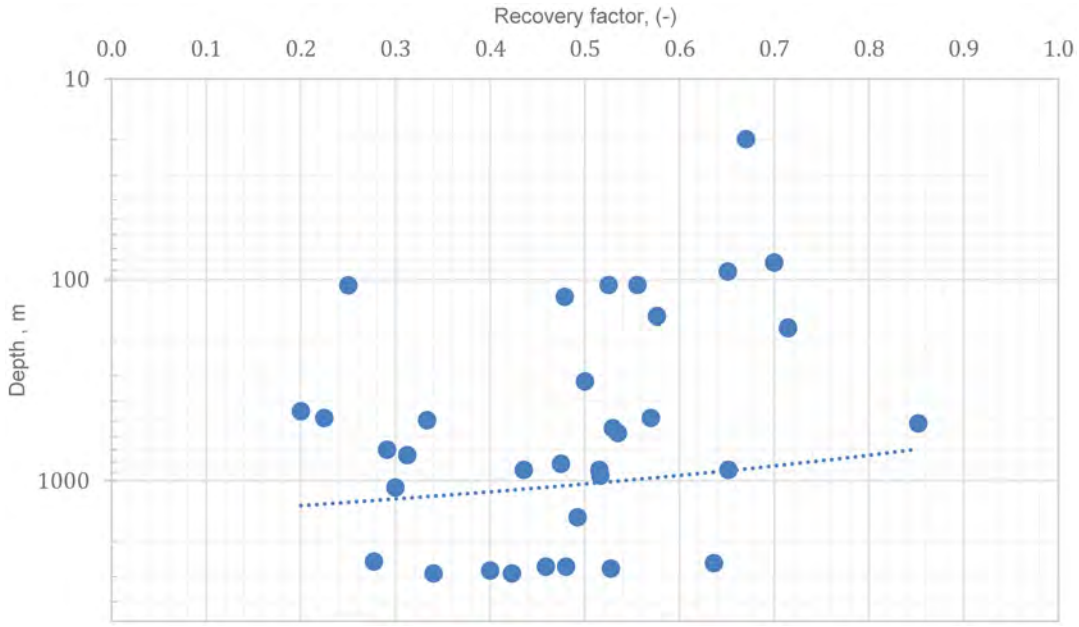

Figure 4—Recovery factor vs. reservoir depth for ISC projects around the world (Koottungal, 2014).

In this preliminary exploring study a series of experimental runs are applied on a real unextracted unconsolidated core sample from Romashkinskoye oilfield. The viscosity of Romashkinskoye crude is around 600,000cP at reservoir conditions. Different recovery schemes are tested experimentally and sequentially in one experimental run, namely: water flooding, hot water flooding, steam flooding, and finally in-situ combustion (ISC). The main target of this study is to evaluate different recovery schemes of Romashkinskoye oil which is characterized by high viscosity and density at reservoir conditions.

The rest of this paper is organized as follows. In section 2, methods are explained which include core sample preparation, experimental set up, and experimental procedure. The experimental results are shown in section 3. Building a numerical model corresponds to lab scale model is presented in section 4. The results of the numerical experiments are presented briefly in section 5 before finally a conclusion of this extensive research is derived in section 6.

Methods

In this section we will describe sample preparation, the experimental setup and experiment procedure.

Sample preparation

The experiment was carried out to determine the flood displacement efficiency by cold-water, hot-water, steam injection and in-situ combustion on sand packed tube of unextracted core. The original core sample is obtained from well's № 300019 of the Oykino-Altuninsky uplift of the Romashkinskoye oilfield. The core was selected from an interval of 72-87 m. The sample consists of sandstone of brown uniform, fine-grained, poorly cemented, intensely oil-saturated with pyrite nodules (diameter 0.5-1 cm). Initial core was used for creating sandpack for the experiment. The original core was grinded to a grain size of 0.1 ÷ 1 mm (Figure 5). The grinded rock was thoroughly mixed and pressed into the core holder by a plunger.

Figure 5—(a) Initial full size core, (b) grinded core (gain size 0.1 ÷ 1 mm).

The initial oil saturation was determined using two methods. The saturation by weight is S_{oi}=9.10% (% weight by extraction) and S_{oi}=9.68% (% weight by thermogravimetry (TG)).

Experimental set up

The laboratory setup for determining the oil displacement efficiency during the whole experiment consists of an agent supply system, high-pressure chamber, fluid collection system, and pressure and temperature measurement and control system (Figure 6). This laboratory setup is described in details in the articles (Minkhanov et al., 2020; Minkhanov et al., 2021; Varfolomeev et al., 2021).

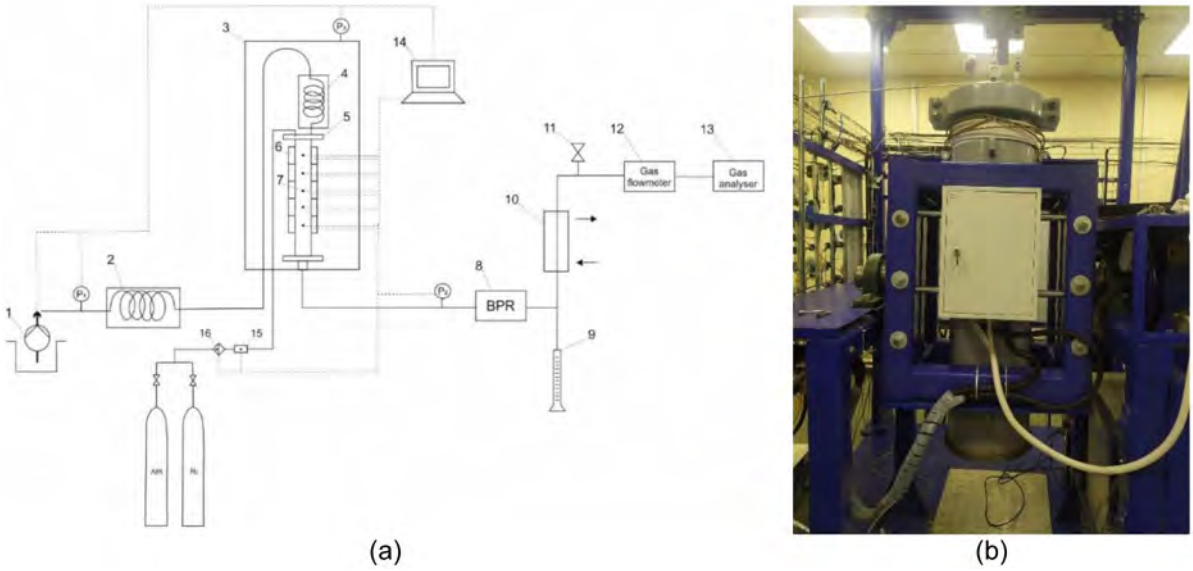

Figure 6—(a) Schematic of steam injection and in-situ combustion apparatus and it consists of 1) Plunger pump; 2) Steam generator; 3) High pressure chamber; 4) Internal steam generator; 5) Core holder; 6) Ring heater; 7) Thermocouple; 8) Back pressure regulator; 9) Separation burette; 10) Condenser; 11) Valve; 12) Gas flowmeter; 13) Gas analyzer; 14) Data logger; 15) Flow meter; 16) Air filter, (b) photo of the high pressure chamber.

The core holder is a cylindrical steel pipe with a length of 34 cm and an inner diameter of 50 mm with fittings for axial thermocouples with a flange type of fastening (Figure 7).

Figure 7—Core holder.

Thermocouples are assembled in accordance with the scheme in Figure 8. The main axial thermocouples T2 – T6 are located in the center of the core with an offset of 5 cm. They record the real-time temperature of the core during the experiment. Thermocouples T12 – T16 are located under the heaters for temperature control to maintain adiabatic condition of the core holder.

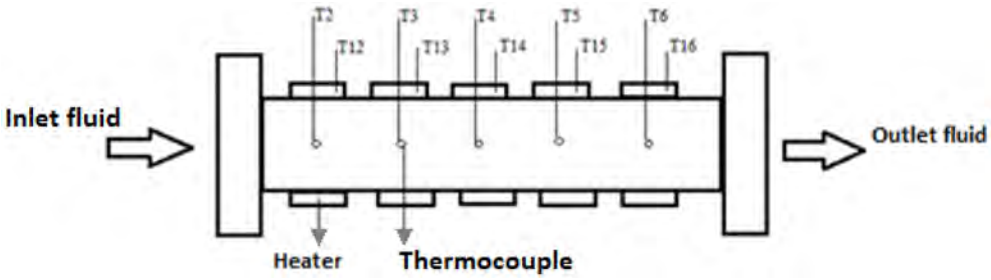

Figure 8—Schematic of the core holder with locations of thermocouples and heaters.

Experimental procedure

Detailed properties of the sandpack model are given in table 2.

Table 2—The main parameters model of the experiment

Parameters	Value
Model length	34 cm
Inner diameter	50 mm
Sand+ oil model weight	1 104,4 g
Initial oil saturation (determined by extraction)	9.10%
Initial oil saturation (determined TG)	9.98%
Initial permeability before the experiment	29 D
Permeability after the experiment	34 D
Porosity	33 %

The experiment was carried out in four stages with different durations (Table 3).

Table 3—Experiment Parameters

№	Experiment stage	Flow rate, ml/min	Temperature, °C	Pressure, MPa	Duration, Pore volume
1	Cold water	3	23	0.5	2
2	Hot water		100		3
3	Steam		200		5
4	In-situ combustion	3000	Max 800°C		To complete the combustion

The effluent collection system consisted of a back pressure regulator, which ensured the reservoir pressure was maintained in the model and the fluid was withdrawn to the separation burette, where separation under standard conditions for liquid and gas took place. Gas entered the gas analyzer to determine the composition of the gas. The dynamics of the filtration of the produced fluid in the separation burette was determined.

Precision pressure sensors were installed at the inlet and outlet of the model and reflected the pressure change in real time. Ring ceramic heaters are installed along the core holder to prevent heat loss during the experiment.

Experimental results

The results of the lab experiment are presented in figures 9 through 14 and tables 4 and 5.

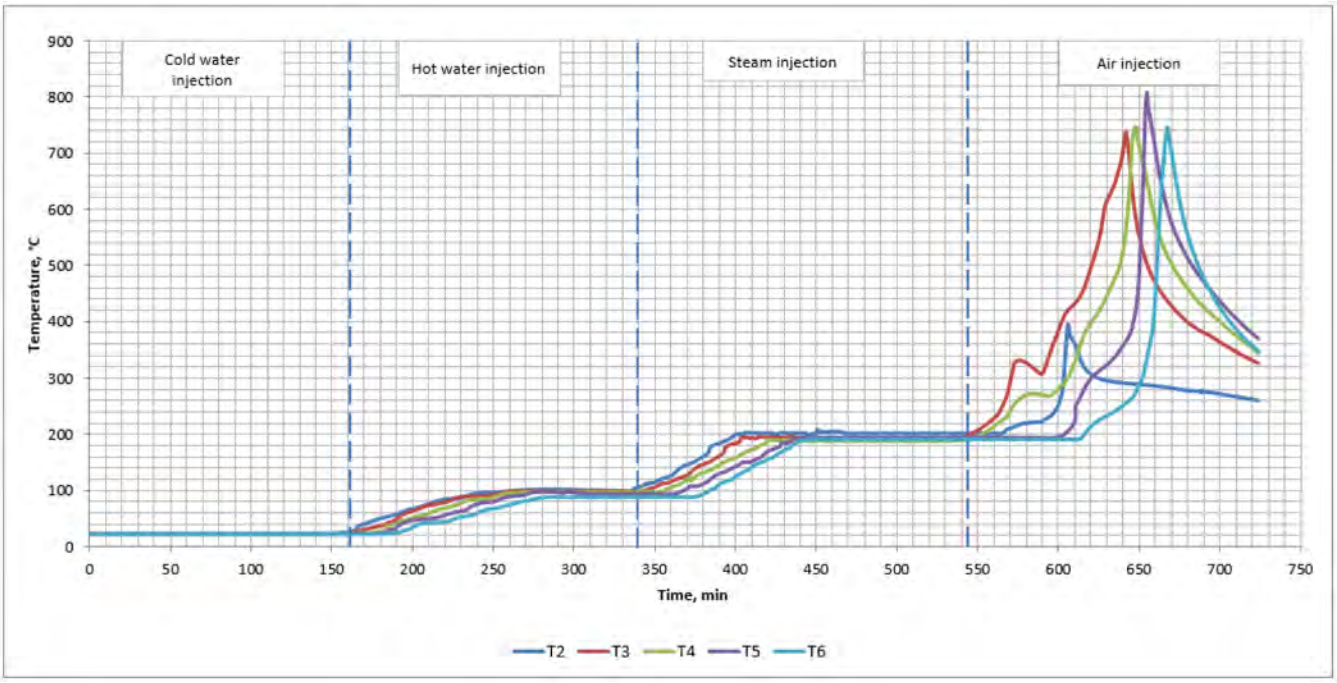

Figure 9—Temperature history of each zone for the experiment.

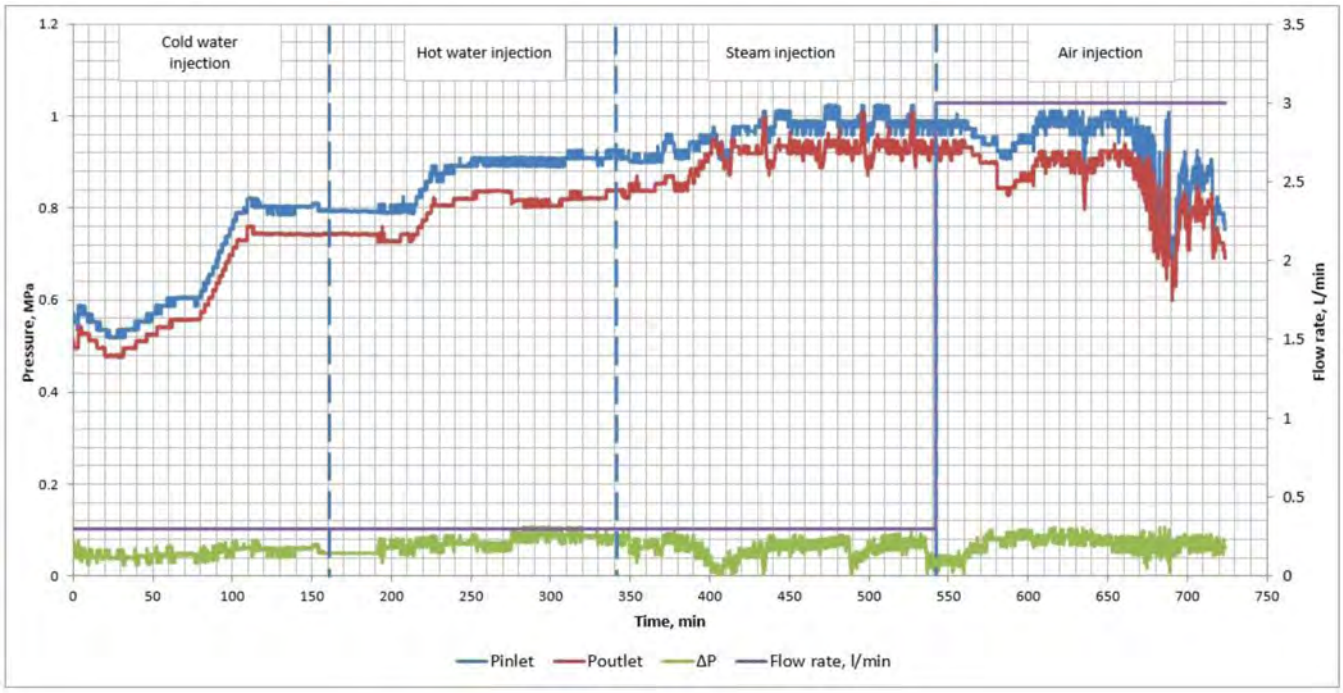

Figure 10—Profile of inlet and outlet pressures, differential pressure, and flow rate.

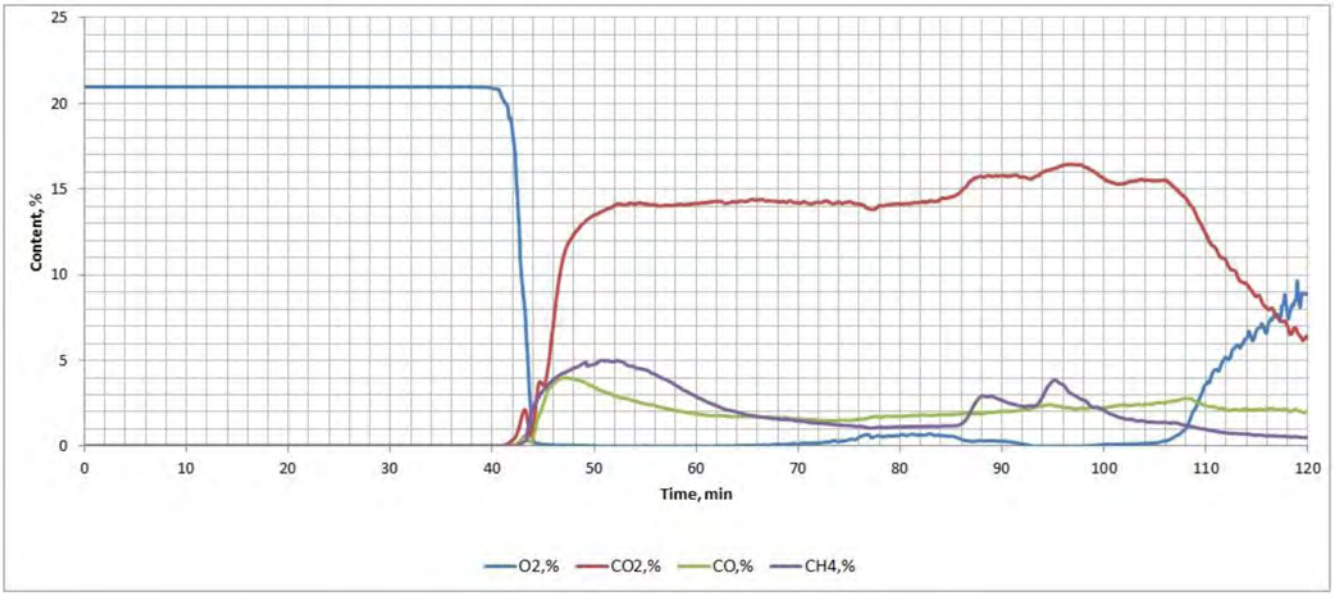

Figure 11—Composition of effluent gas.

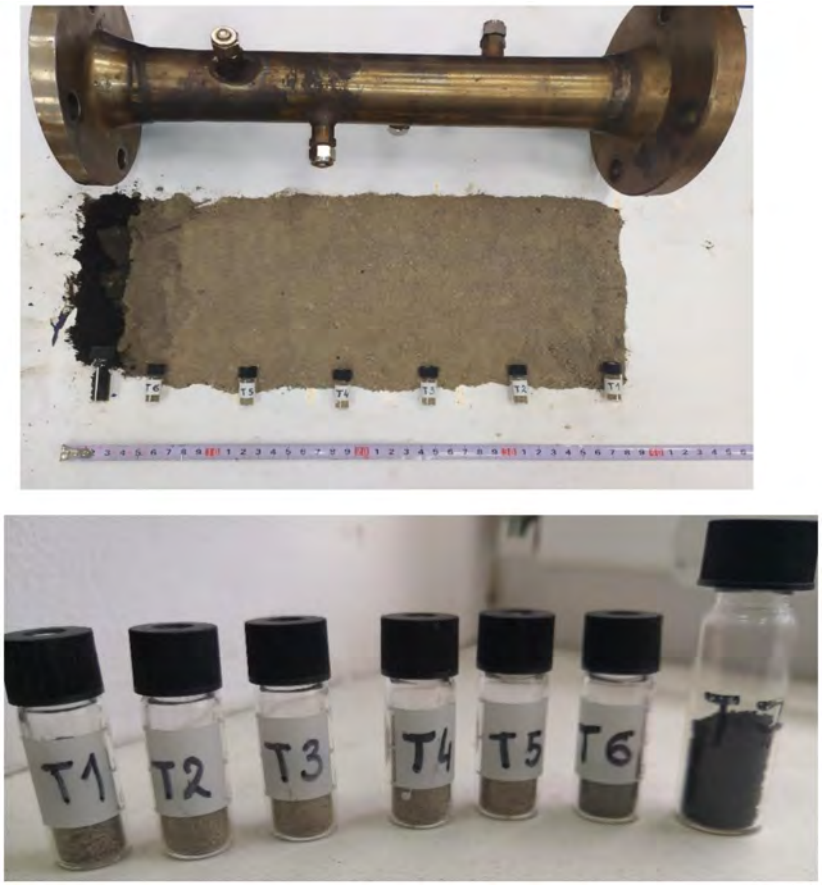

Figure 12—Appearance of post combustion sands.

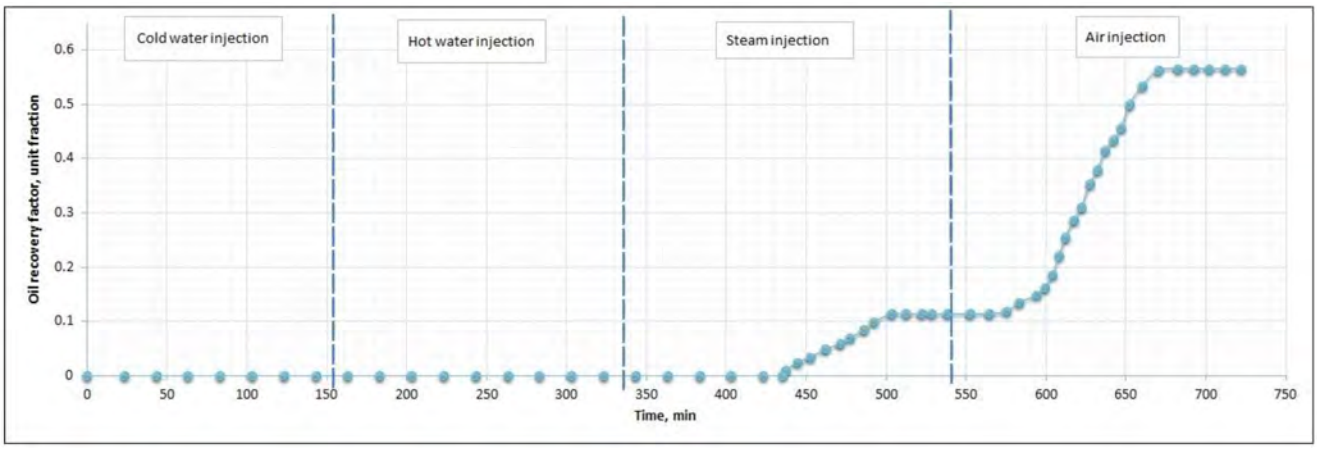

Figure 13—Dynamics of oil displacement efficiency.

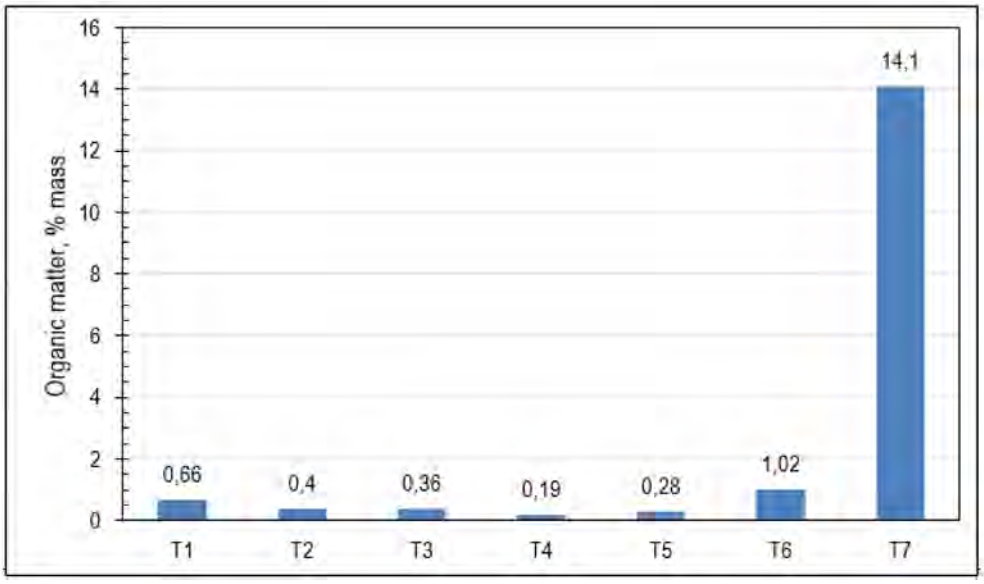

Figure 14—Dynamics of changes of the organic matter contents at points T1-T7 of the core model.

Table 4—Material balance after the experiment

№	Injected agent	According to extraction	According to TG
		Oil displacement efficiency, % mass	Organic matter, % mass
1	Water	0	T1 = 0.66 T2 = 0.40 T3 = 0.36 T4 = 0.19 T5 = 0.28 T6 = 1.02 T7 = 14.10
2	Hot water	0	
3	Steam	11.48	
4	ISC	45.08	
Total		56.56	

Table 5—Properties of the initial and recovered oil during the experiment - SARA analysis, elemental analysis and viscosity

Composition, characteristics	Initial oil before treatments	Recovered oil obtained after steam injection	Recovered oil obtained after ISC
	Group composition, %		
Saturates	29.38	72.72	54.16
Aromatics	17.59	16.86	27.76
Resins	31.99	4.59	12.54
Asphaltenes	21.04	5.83	5.54
Viscosity, mPa·s (25 °C)	260100	21.2	557.2

Water was injected at room temperature (23 °C) in the amount of two pore volumes. When injecting hot water the temperature reached to 102 °C while in steam flooding the temperature was 200 °C. The ignition occurred at about 200 °C. Maximum temperature at air injection was 808 °C (Figure 9).

According to the gas profile data, the CO_2 content of the effluent gas mixture is 14-15% (stable values over the entire interval), the maximum CO_2 value is 16.5%, which indicates a stable combustion front.

Sand packed tube was removed for post combustion analysis. Samples were taken at locations T1-T7 (every 6 cm) as illustrated in figure 12.

At the stages of cold water and hot water injection, no oil effluent was received (figure 13). Steam flooding achieved a recovery of 11.48 %. Air injection was carried out at temperature 200 °C directly after steam flooding. A stable combustion front was observed with oil displacement efficiency equals 45.08% (recovery factor). Water injection is ineffective for this oil in spite of significant viscosity reduction at 100 °C during hot water flooding. Total oil displacement efficiency 56.56 % is achieved (Figure 13 and table 4).

Total organic matter content was analyzed by TG. Figure14 presents dynamics of the organic matter content at locations T1-T7 of the core model. In the first six zones, only a small amount of the organic matter was left after the experiment. In the seventh zone, the content of organic matter reached 14%. This is consistent with the color of post-tested sand (Figure 12).

After visual inspection of the color changes of the sand and analysis of the TG data, it is possible to draw conclusions about a stable oil displacement front during ISC.

The produced oil in the steam injection process was a result of significant reduction in the viscosity and stripping of light components from the oil. However, the recovery factor was very low compared to reported data in the literature for steam flooding. In ISC process, the oil recovery was mainly due to upgrading of heavy components (Table 5).

Analysis of SARA fractions indicates an increase in the content of saturates from 29.38% to 72.72% (after steam injection) and 54.16% (after ISC) with a decrease in the content of resins and asphaltenes. The content of asphaltenes was reduced by about 72–74%, which partly proves that the widely accepted opinion that asphaltene is the main source of fuel (coke) for the combustion (Yuan et al., 2018; Liu et al., 2020). It is believed that the in-situ upgrading of heavy oil is associated with the favorable conditions for hydrogen generation in water gas shift reactions and coke gasification reactions due to the oxygen deficiency (Turta et al., 2020).

Numerical modelling

The simulation has been done using the thermal simulator CMG-STARS (CMG-STARS, 2020). The whole experimental procedure is simulated using 1D vertical model corresponds to the laboratory size of the combustion tube. The original combustion tube cell is a cylindrical-shaped and first we have tried to model it in the original shape but from our experience the Cartesian rectangular shape is more efficient for ISC due to the simple geometrical symmetry while the cylindrical geometry is more complex and the grid cells are not equally distributed along the simulated domain which will increase the simulation time due to the nature of combustion front.

Geometry and boundary conditions

The simulated model is 1D vertical rectangular-shape domain which corresponds in size to the cylindrical combustion tube cell. The length is kept the same as the original cell size 34cm and based on that the size of gridblock is calculated. Figure 15 illustrates the built model with dimensions. The injection well is placed in the central block at the top of the model while the production well is placed on the opposite side as can be seen from figure 15. The fluid injection rates and bottom whole pressure (BHP) are the two constraints for the injection and production wells through the whole numerical simulation. The applied values are retrieved from figure 10 for each stage. The maximum pressure allowed is 10.5 bar. The maximum rates are taken from table 3.

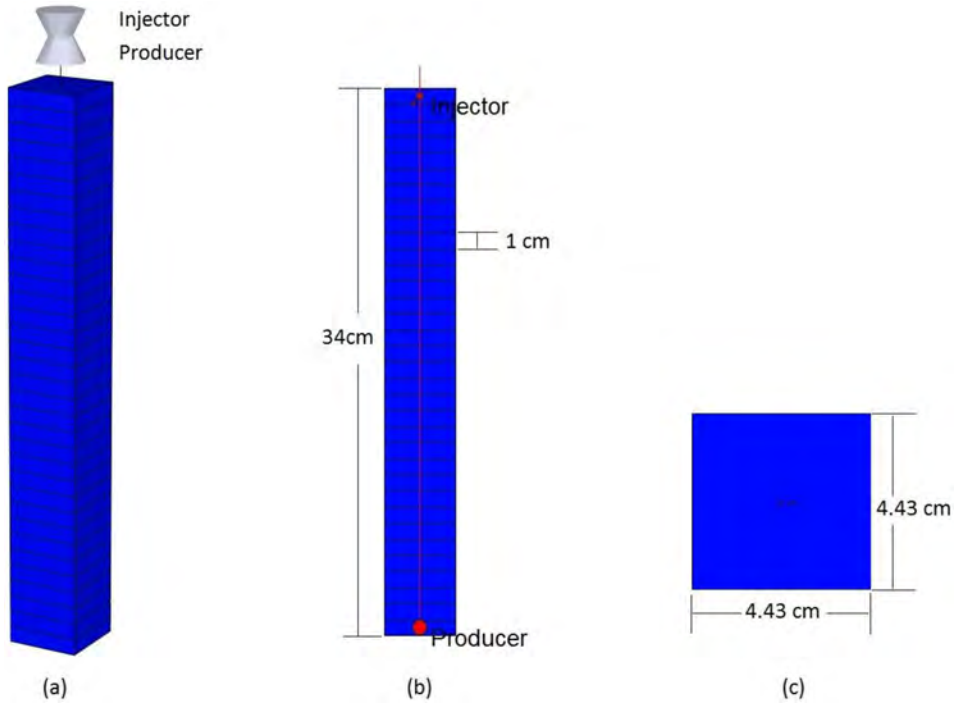

Figure 15—(a) 1D (3D view) Cartesian simulation model, b) IK view of the model with injection and production wells locations, and (c) IJ (aerial) view of the model.

Grid sensitivity analysis

From our experience the gridlocks' size that is chosen in this study is sufficient for the normal flooding processes like water and steam. However, ISC is a special process where a combustion front propagates slowly inside the porous medium and the kinetics of reactions may depend also on the gridblock size. Many researchers reported on the effect of gridblock size on the accurate resolution of the ISC model. The combustion front thickness has been reported by (Bagci, 1998) to be in the range 2.5 to 8.9cm. (Belgrave et al, 1993) reported in there results a combustion front thickness between 7 to 10cm. (Yang and Gates, 2009) used a very fine gridblock size to resolve the model adequately and they reported on a gridblock size ranging from 2.5 to 10mm. In this study the gridblock thickness of 10mm found to be fine enough to obtain adequate results for ISC run.

Rock and fluid properties

The numerical model requires rock and fluid properties to be furnished in the already built gridblocks model (Tables 6 and 7). Flow and temperature conditions of the complete sequence of experiments are listed in table 8. As it has been stated in the experimental part that the combustion tube was under adiabatic conditions, therefore heat losses during numerical experiments were considered to be zero. Viscosity data against temerature were obtained experimentally. The values are listed in table 9. Figure 16 illustrates the viscosty change with temperature graphically.

Table 6—Rock properties

Rock compressibility (1/kPa)	$1.45e^{-7}$
Rock thermal conductivity (W/m.°C)	2.767
Rock heat capacity (J/kg. °C)	818
Rock density (kg/m^3)	1950
Thermal expansion coefficient (1/°C)	7.2e-5

Table 7—Oil properties

Density (kg/m^3)	990
Bitumen thermal conductivity (W/m.°C)	0.112
Bitumen average heat capacity (J/kg.°C)	1200
Volumetric thermal expansion (1/°C)	7.2e^{-4}
Bitumen compressibility (1/kPa)	3.78e^{-5}

Table 8—Experiment conditions

Parameters	**Value**
Pressure (kPa)	500-1100
Q water injection	3 ml/min
Q steam injection	3 ml/min
Q air injection	3 L/min
Steam temperature (°C)	200
Steam quality (%)	100
Steam injection pressure(kPa)	500
ISC ignition temperature (°C)	200

Table 9—Viscosity of oil vs. temperature

Temperature, °C	**Viscosity, mPa * s (cP)**	
	Initial oil	**Oil after air injection**
20	606550.00	3403.50
30	125810.00	500.32
40	35621.00	132.21
50	8054.30	62.38
60	2657.90	47.84
70	1130.60	33.19
80	563.80	22.78
90	323.83	13.56
100	201.24	16.17
110	138.93	10.99
120	101.12	14.82
130	92.81	19.31
140	85.85	At 130 °C start to boil a little bit
150	57.56	-
160	40.02	-
170	36.29	-
180	28.46	-
190	36.02	-
200	27.89	-

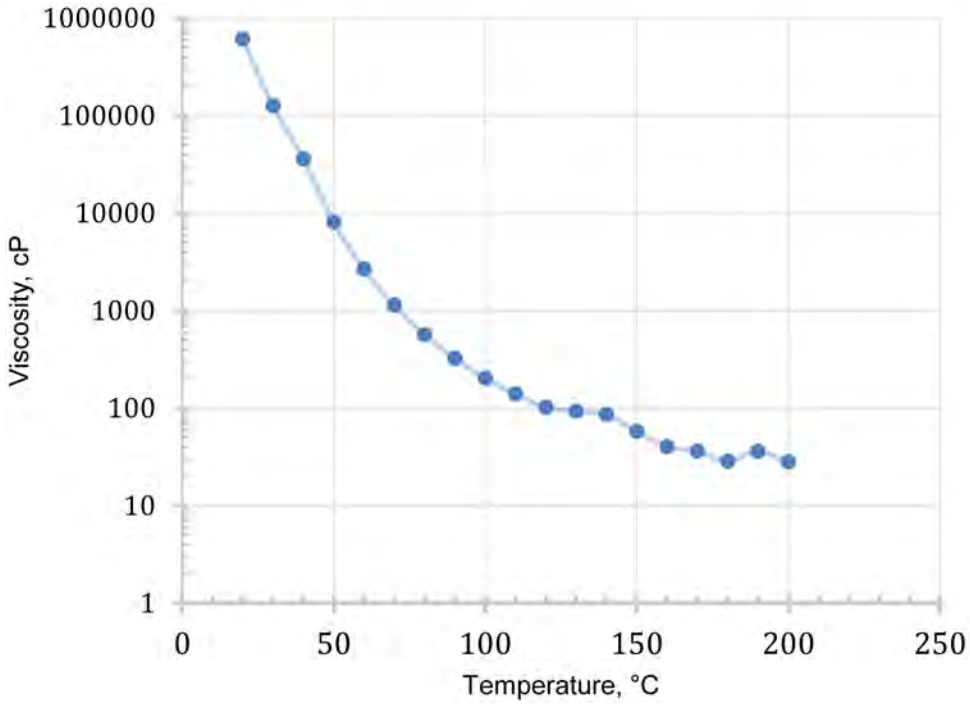

Figure 16—Oil viscosity vs. temperature.

Relative permeability data

The relative permeability data are obtained from the literature (Coats et al., 1974). Two sets of two-phase relative permeability data are used to calculate the three phase relative permeability of oil using stone's second model embedded in CMG-STARS (CMG-STARS, 2020). However, the three-phase relative permeability of oil had to be adjusted to match the steam flooding experiment and used later for combustion tube experiments. The reason is, there were measured values for the porosity and absolute permeability and the only parameter to match the experiment results was the relative permeability for steam flooding case. Relative permeability data are listed in table 10. The effect of temperature on relative permeability was not taken into account in this study.

Table 10—Relative permeability data (water-oil) & (gas-oil) (Coats et al., 1974)

S_w	k_{rw}	k_{row}	S_L	k_{rg}	k_{rog}
0.13	0.0	1	0.2	0.17	0.0
0.191	0.0051	0.999	0.395	0.12	0.0294
0.25	0.0102	0.769	0.433	0.1022	0.0461
0.294	0.0168	0.7241	0.515	0.0855	0.0883
0.357	0.0275	0.6206	0.569	0.0761	0.1172
0.414	0.0424	0.504	0.614	0.0654	0.1433
0.49	0.0665	0.3714	0.663	0.05	0.1764
0.557	0.097	0.3029	0.719	0.0372	0.217
0.63	0.1148	0.1555	0.750	0.0285	0.2255
0.673	0.1259	0.0956	0.805	0.0195	0.2919

PVT model

PVT model is built using WINPROP module (CMG-WINPROP, 2020). Data for model components are obtained from (Belgrave et al., 1993) and listed in table 11. WINPROP built-in data are used for gas-liquid K-values, and gas and liquid heat capacities. These data are listed in tables 12 through 14.

Table 11—Data for model components in WINPROP (Belgrave et al. 1993)

Component	Molecular weight (g/mol)	T_c(°C)	P_c(kPa)
Maltenes	407	619	1480
Asphaltenes	1090	904	792
Coke	13.1	-	-
Water	18.0	374	22.1
O_2	32.0	-119	5050
Gas	43.2	21.9	7180
CH_4	16.0	-82.6	4600
CO_2	44.0	31.1	7380
CO	28.0	-140	3490
N_2	28.0	-147	3390

Table 12—Gas-liquid K-value, $K= (k_{v1}/P)e^{(k_{v4}/(T-K_{v5}))}$ (CMG, 2021)

Component	k_{v1}	k_{v4}	K_{v5}
Maltenes	1.89×10^{7}	-6560	-80.1
Asphaltenes	0	0	0
Water	1.18×10^{7}	-3820	-227
Gas	8.62×10^{8}	-3100	-273
CH_4	5.45×10^{5}	-879	-266
CO_2	8.62×10^{8}	-3100	-273
CO	3.32×10^{5}	-530	-260

Table 13—Gas heat capacity; C_{pg} (J/gmol °C)$=C_{pg1}+C_{pg2}T+C_{pg3}T^2+C_{pg4}T^3$ (CMG, 2021)

Component	C_{pg1}	C_{pg2}	C_{pg3}	C_{pg4}
Maltenes	0	0	0	0
Asphaltenes	0	0	0	0
O_2	28.1	-3.68×10^{-6}	1.75×10^{-5}	-1.06×10^{-8}
Gas	19.8	7.34×10^{-2}	-5.60×10^{-5}	1.71×10^{-8}
CH_4	19.3	5.21×10^{-2}	1.20×10^{-5}	-1.13×10^{-8}
CO_2	19.8	7.34×10^{-2}	5.60×10^{-5}	1.71×10^{-8}
CO	30.9	-1.29×10^{-2}	2.79×10^{-5}	-1.27×10^{-8}
N_2	31.2	-1.36×10^{-2}	2.68×10^{-5}	-1.17×10^{-8}

Table 14—Liquid heat capacity, C_{pl} (J/gmol °C) $=C_{pl1}+C_{pl2}T+C_{pl3}T^2+C_{pl4}T^3$ (CMG, 2021)

Component	C_{pl1}	C_{pl2}	C_{pl3}	C_{pl4}
Maltenes	994	0	0	0
Asphaltenes	2510	0	0	0
O_2	46.4	3.95×10^{-1}	-7.05×10^{-3}	3.99×10^{-5}
Gas	-3980	5.25×10^{-1}	-2.27×10^{-1}	3.29×10^{-4}
CH_4	-0.02	1.20	-9.87×10^{-3}	3.17×10^{-5}
CO_2	-3980	5.25×10^{-1}	-2.27×10^{-1}	3.29×10^{-4}
CO	126	-1.70	1.07×10^{-2}	4.19×10^{-6}
N_2	76.5	-3.52×10^{-1}	-2.67×10^{-3}	5.01×10^{-5}

Reaction model

The literature is rich with reaction models for different types of oil (light and heavy). The most famous schemes to model heavy oil and bitumen reactions during ISC process is to allow for thermal cracking, low thermal oxidations (LTO), and high thermal oxidations (HTO). In this study, the model of (Belgrave et al, 1993) will be considered after testing several models. For more information on the reaction modelling of ISC one can review (Belgrave et al., 1993; Jia et al., 2005; Yang, 2019; Mokheimer et al., 2019). (Belgrave et al, 1993) model reads:

Thermal cracking reactions (first order).

$$Maltenes \rightarrow 0.372 \quad Asphaltenes \tag{1}$$

$$Asphaltenes \rightarrow 83.223 \quad Coke \tag{2}$$

$$Asphaltenes \rightarrow 37.683 \quad Gas \tag{3}$$

LTO reactions.

$$Maltenes + 3.431 \quad O_2 \rightarrow 0.4726 \quad Asphaltenes \tag{4}$$

$$Asphaltenes + 7.513 \quad O_2 \rightarrow 101.539 \quad Coke \tag{5}$$

HTO reactions.

$$Coke\left(CH_{1.3}\right) + 1.232O_2 \rightarrow CO_x + 0.565H_2O \tag{6}$$

Another group of reactions is considered for completeness of the ISC model and suggested by (Yang and Gates, 2009).

Gas phase combustion.

$$Methane + 2O_2 \rightarrow CO_2 + 2H_2O \tag{7}$$

$$Gas + 2O_2 \rightarrow 0.9695 \quad CO + CO_2 + 2H_2O \tag{8}$$

The kinetic data of reactions is retrieved from (Belegrave et al., 1993) and is listed in table 15.

Table 15—Kinetic data of reactions (Belgrave et al., 1990)

Reaction	A	E_a(J/mol)	H_r(J/mol)
1	9.09×10^{12} s^{-1}	2.35×10^5	0
2	4.06×10^9 s^{-1}	1.77×10^5	0
3	1.36×10^9 s^{-1}	1.76×10^5	0
4	6.82×10^3 s^{-1} $Pa^{-0.4246}$	8.67×10^5	1.30×10^6
5	2.13×10^{-10} s^{-1} $Pa^{-4.7627}$	1.86×10^5	2.86×10^6
6	1.07×10^{-11} s^{-1} Pa^{-1}	3.48×10^5	4.28×10^5

To set the stoichiometry of HTO reaction, the experimental data are analysed using (Sarathi, 1999) approach and for the sake of abbreviation, we will not detail the approach here. The final reaction of combustion (HTO) reads (Nassan, 2021),

$$Coke\left(CH_{1.26}\right) + 1.283\left(O_2 + 3.76N_2\right) \rightarrow 0.875CO_2 + 4.82N_2 + 0.125CO + 0.6314H_2O + 0.0298O_2$$

History matching

History matching primary goal is to match oil and gas production volumes, injected water, steam and air rates, pressure, and temperature change during the experiment. As there were no oil production during cold and hot water injection, the initial model parameters were left without any change because the oil was not movable due to high viscosity. For steam injection, the only parameter that was manipulated was relative permeability. Capillary pressure was neglected in this study as it is a preliminary study and capillary pressure can be considered in further investigations. To history match ISC experiments, kinetic data were manipulated in terms of frequency factor (A), activation energy (E_a), and heat of reaction (H_r). The kinetic data after history match are listed in table 16.

Table 16—Kinetic data of reactions from history matching

Reaction	A	E_a(J/mol)	H_r(J/mol)
1	6.2×10^{14} s^{-1}	1.23×10^4	0
2	2.4×10^6 s^{-1}	2.06×10^5	0
3	8.1×10^{13} s^{-1}	6.20×10^4	0
4	6.82×10^8 s^{-1} $Pa^{-0.4246}$	3.5×10^5	2.4×10^6
5	3.05×10^6 s^{-1} $Pa^{-4.7627}$	1.2×10^5	2.25×10^5
6	1.35×10^4 s^{-1} Pa^{-1}	2.3×10^3	4.1×10^5
7	3.80×10^9 s^{-1} Pa^{-1}	3.6×10^5	8.1×10^6
8	2.20×10^{11} s^{-1} Pa^{-1}	5.7×10^5	6.3×10^5

Numerical results and future work

To run all numerical experiments on the same model, a restart file was generated after each run. For the sake of abbreviation we will show recovery curve of the four experiments which can be seen in figure 17. The match of numerical model and experiment in steam flooding process is good. However, the match of ISC combustion was not an easy task and it can be seen that the match is not as good as in steam flooding. The recovery factor in ISC was always higher than the actual measured value. The final recovery of ISC was about 3 % higher than the measured recovery factor.

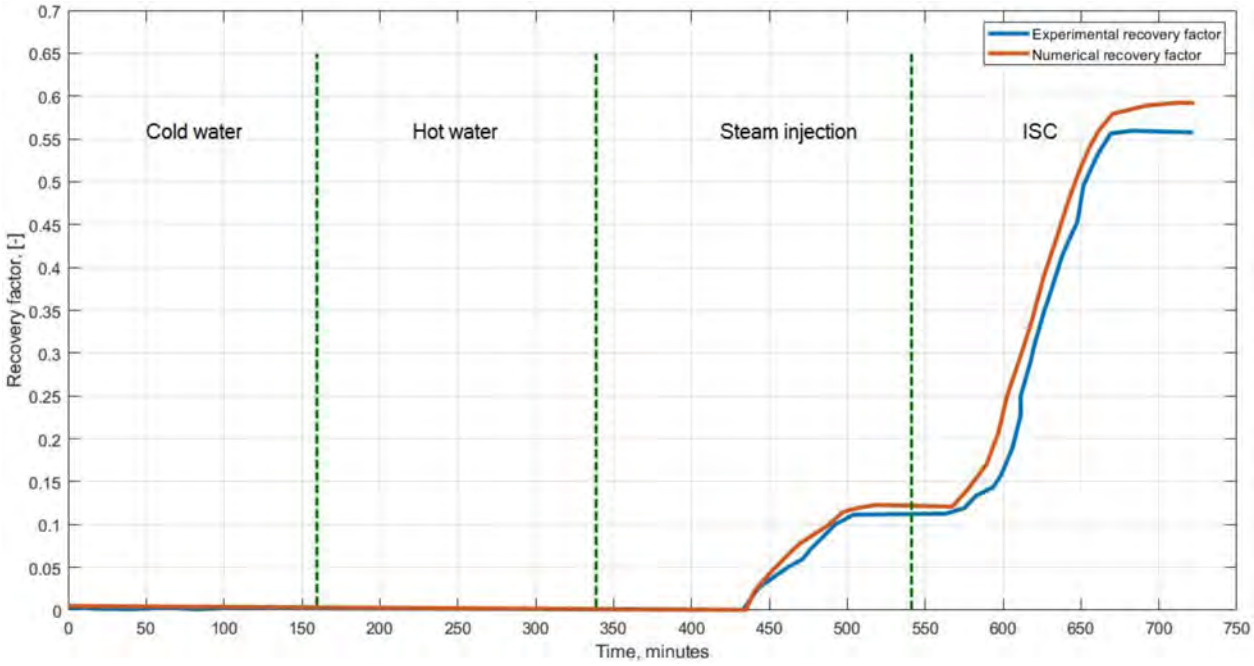

Figure 17—Comparing recovery curves of the complete lab and numerical experiments.

Figure 18 shows the temperature change at the gridblocks which correspond to the thermocouples locations in the lab experiment (T2-T6). Gridblocks (1,1,8), (1,1,13), (1,1,18), (1,1,23), and (1,1,28) correspond to five thermocouples (T2, T3, T4, T5, T6) that were used to produce the curves in figure 19 experimentally. Figures 18 and 19 can be compared and they match each other with slightly higher temperature in figure 18 which justify the high recovery factor in the numerical run compared to the lab run. Table 17 compares the produced gas from numerical and lab experiments. Methane is not produced in the numerical model which confirms the need for further enhancement of the model. This enhancement can be achieved by running more lab experiments and developing the numerical model by testing more reaction models which will be the next step in future experiments. The reaction model need to include more reactions to allow for CH_4 fractions to appear in the flue gas. The final lab-size numerical model can be used to develop a field-scale numerical model which will be in the favour of commercial development of Romashkinskoye oilfield.

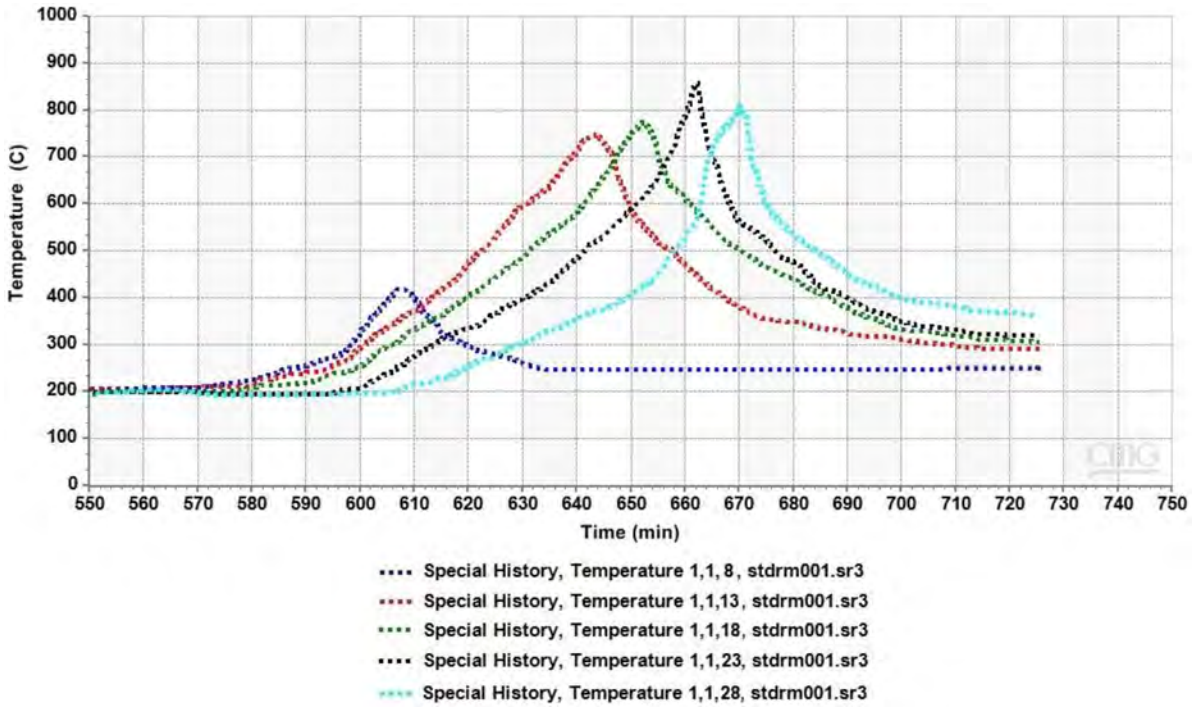

Figure 18—Temperature distribution in the combustion tube during ISC in the numerical model at different gridblocks which correspond to the thermocouples locations in the lab experiment.

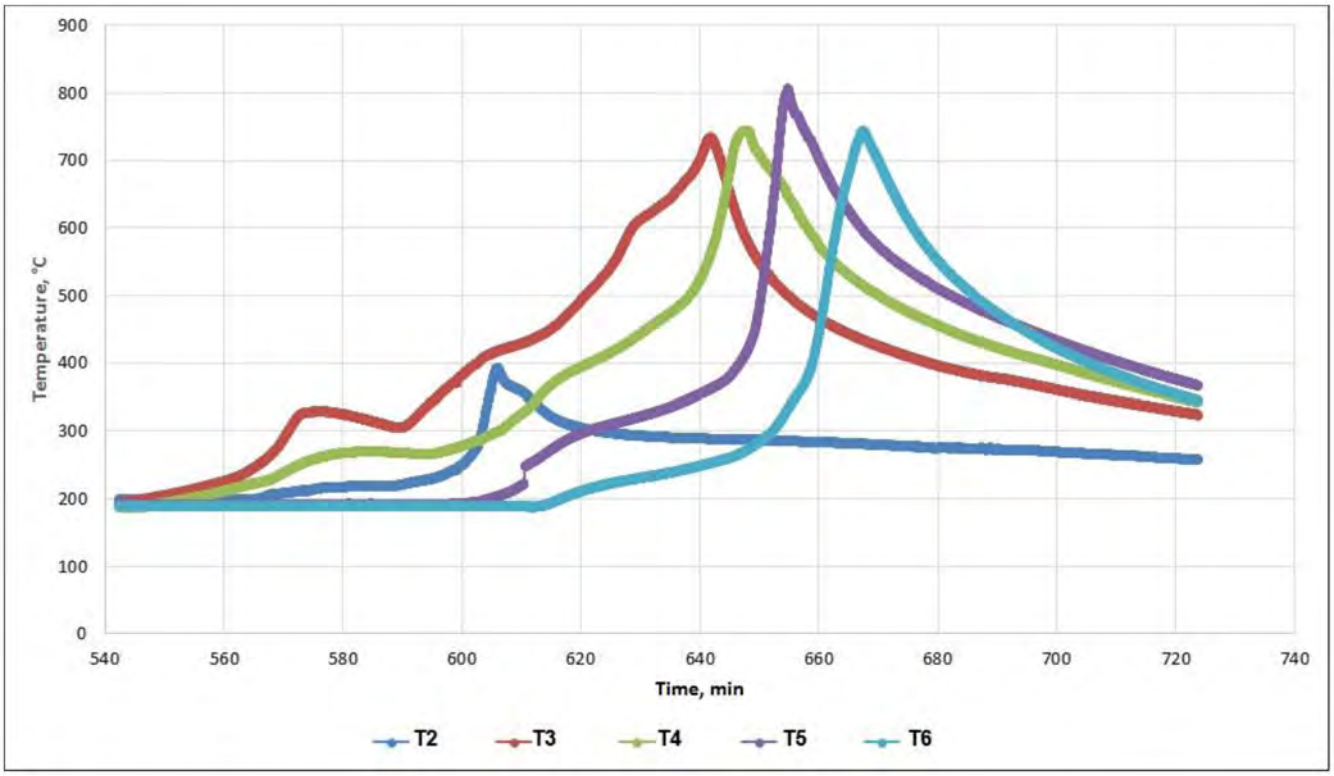

Figure 19—distribution in the combustion tube during ISC in the lab experiment.

Table 17—Average effluent gas composition (%)

Component	Experiment	Simulation
CO_2	14.96	16.22
CO	1.94	2.84
CH_4	1.87	0.00
O_2	0.26	0.15
N_2	81.02	80.7

Conclusions

A comprehensive experimental and numerical simulation are implemented on a crushed original core from Romashkinskoye oilfield located in Russia. The viscosity of the crude oil is above 600,000 cP. Different EOR schemes are tested experimentally and numerically, namely; cold water flooding, hot water flooding, steam flooding, and finally ISC. The following results can be drawn from this preliminary study:

- On contrary to what was expected hot water didn't achieve any recovery from the sample in spite of considerable viscosity reduction;
- Steam injection recovered only 11.5% of original oil which is very low compared to reported data in the literature;
- Initial evaluation of the ISC process showed a stable combustion front which proves that ISC is feasible for Romashkinskoye oil where resins and asphaltenes form about 50% wt of the crude oil;
- The results of numerical modeling of water, hot water, and steam flooding were in good agreement with the experimental results while the in-situ combustion simulation showed a better recovery factor than experiments;
- The laboratory and numerical experiments will improve our understanding of the recovery options of Oykino-Altuninsky uplift of the Romashkinskoye oilfield and help the developers to choose the best production sequence for this oilfield after running more lab experiments on unconsolidated and consolidated cores which are under preparation;
- The lab experiments will provide inputs for the field-size numerical model.

Acknowledgements

This work was supported by the Russian Science Foundation (project code № 21-73-30023).

Nomenclature

A	Frequency factor
API	American Petroleum Institute gravity
C_p	Heat capacity, J/gmole. °C
E_a	Activation energy, (J/mol)
H_r	Heat of reaction, (J/mol)
K	Gas-liquid equilibrium value
k_{rg}	Gas relative permeability
k_{rog}	Oil relative permeability in gas-oil system
k_{row}	Oil relative permeability in oil-water system
k_{rw}	Water relative permeability
S_L	Liquid saturation (water + oil), %
S_w	Water saturation, %

P Pressure, kPa
P_c Critical pressure, kPa
T Temperature, °C
T_c Critical temperature, °C
TG Thermogravimetry

Subscript

g Gas
o Oil
w Water

References

Al-Muntaser, A. A., Varfolomeev, M. A., Suwaid M. A., Yuan, C., Chemodanov A. E., Feoktistov D. A., Rakhmatullin I. Z., Abbas M., Domínguez-Álvarez E., Akhmadiyarov A. A., Klochkov V. V., and Amerkhanovd M. I. 2020. Hydrothermal upgrading of heavy oil in the presence of water at sub-critical, near-critical and supercritical conditions. *Journal of Petroleum Science and Engineering* **184**(1):106592. https://doi.org/10.1016/j.petrol.2019.106592.

Al-Murayri, M. T., Maini, B. B., Harding, T. G., and Oskouei, J. 2016. Multicomponent solvent co-injection with steam in heavy and extra-heavy oil reservoirs. *Energy Fuels* **30** (4): 2604-2616. https://doi.org/10.1021/acs.energyfuels.5b02774.

Alboudwarej, H., Felix, J., Badry, R. et al. 2006. Highlighting heavy oil. *Oilfield review*, Schlumberger. https://www.slb.com/-/media/files/oilfield-review/heavy-oil-2-englsh.

Arcelus-Arrillaga, P., Pinilla, J. L., Hellgardt, K., and M. Millan. 2017. Application of water in hydrothermal conditions for upgrading heavy oils: A review. *Energy Fuels* **31** (5): 4571-4587. https://doi.org/10.1021/acs.energyfuels.7b00291.

Bagci, S. 1998. Estimation of combustion zone thickness during in-situ combustion processes: *Energy Fuels*, **12**(6): 1153–1160. https://doi.org/10.1021/ef980013m.

Belgrave, J. D. M., Moore, R. G., Ursenbach, M. G., and Bennion, D. W. 1993. A comprehensive approach to in situ combustion modeling. *SPE Advanced Technology Series* **1** (01): 98–107. SPE-20250-PA. https://doi.org/10.2118/20250-PA.

CMG-STARS 2020.10, Computer Modelling Group, User's Guide. 2020. http://www.cmgl.com.

CMG-WINPROP 2020.10, Computer Modelling Group, User's Guide. 2020. https://www.cmgl.com.

Coats, K.H., George, W.D., Chu, C., Marcum, B.E. 1974. Three-dimensional simulation of steamflooding. *SPE J.* **14** (06): 573–592. SPE-4500-PA. https://doi.org/10.2118/4500-PA.

Green, D. W. and Willhite, G. P. 2018. Enhanced oil recovery, Second edition. Richardson, Texas: Society of Petroleum Engineers. ISBN: 978-1-61399-494-8.

Hamedi, Y. S., and Babadagli, T. 2013. In-situ upgrading of heavy oil/bitumen during steam injection by use of metal nanoparticles: A study on in-situ catalysis and catalyst transportation. *SPE Res Eval & Eng* **16** (03): 333–344. SPE-146661-PA. https://doi.org/10.2118/146661-PA.

Jia, N., Moore, R. G., Mehta, S. A., Van Fraassen, K., Ursenbach, M. G., and Zalewski, E. 2005. Compositional changes for Athabasca bitumen in the presence of oxygen under low temperature conditions. *J. Can. Petrol. Technol*. **44**(9):51–57. PETSOC-05-09-06. https://doi.org/10.2118/05-09-06.

Koottungal, L. 2014. Worldwide EOR survey. *Oil & Gas Journal*, Apr 7th. https://www.ogj.com/drilling-production/production-operations/ior-eor/article/17210637/2014-worldwide-eor-survey.

Lake, L. W. 2010. Enhanced oil recovery. Richardson, Texas: Society of Petroleum Engineers. ISBN: 978-1-55563-305-9.

Lake, L. W., Russel T. J., Rossen, W. R., and Pope, G. A. 2014. Fundamentals of enhanced oil recovery. Richardson, Texas: Society of Petroleum Engineers. ISBN: 978-1-61399-328-6.

Liu, D., Zhang, X., Li, G., Kanni, Z., Song, Q., Zheng, R. 2020. Comparative study on the coking characteristics of two low-asphaltene heavy oils and their main fractions. *J. Petrol. Sci. Eng*. **184**(1):106500. https://doi.org/10.1016/j.petrol.2019.106500.

Minkhanov, I. F., Marvanov, M. M., Bolotov, A. V., Varfolomeev, M. A., Khairtdinov, R. K. 2020. Improvement of heavy oil displacement efficiency by using aromatic hydrocarbon solvent. International Multidisciplinary Scientific GeoConference: SGEM 20 : 711-718. http://doi.org/10.5593/sgem2020/1.2/s06.090.

Minkhanov, I. F., Bolotov, A. V., Al-Muntaser, A. A., Mukhamatdinov, I. I., Vakhin, A. V., Varfolomeev, M. A., Slavkina, O. V., Shchekoldin, K. A., and Darishchev, V. I. 2021. Experimental study on the improving the efficiency of oil

displacement by co-using of the steam-solvent catalyst (Russian). Neftyanoe khozyaystvo-Oil Industry 2021, 06: 54-57.

Mokheimer, E. M. A., Hamdy, M., Abubakar, Z., Shakeel, R. M., Mohamed, A. H., Mahmoud, M. 2019. A Comprehensive Review of Thermal Enhanced Oil Recovery: Techniques Evaluation. *J. Energy Resour. Technol*. **141**(3): 030801. https://doi.org/10.1115/1.4041096.

Nassan, T. H. 2021. Numerical modelling of thermal enhanced oil recovery methods. (Unpublished PhD thesis). Technical University Bergakademie Freiberg. Freiberg-Germany.

Nassan, T. H., and Amro, M. M. 2021. Cold waterflooding vs. steam injection applicability for heavy oil reservoirs as a secondary stage recovery method. Presented at European Symposium on Improved Oil Recovery, Vienna, 19-22 April. https://doi.org/10.3997/2214-4609.202133071.

Sarathi, P. S. 1999. In-Situ Combustion Handbook -- Principles and Practices. U.S Department of Energy. https://doi.org/10.2172/3175.

Turta, A., Kapadia, P., Gadelle, C. 2020. THAI process: determination of the quality of burning from gas composition taking into account the coke gasification and water-gas shift reactions. *J. Petrol. Sci. Eng*. **187**(4): 106638. https://doi.org/10.1016/j.petrol.2019.106638.

Varfolomeev, M. A., Yuan, C., Bolotov, A. V., Minkhanov, I. F., Mehrabi-Kalajahi, S., Saifullin, E. R., and Marvanov M. M., Baygildin, E. R., Sabiryanov, R. M., Rojas, A.,Emelianov, D. A., Al-Muntaser, A. A., Ganiev, B. G., Zaripov A. T., Beregovoi, A. N., and Shaihutdinov, D. K. 2021. Effect of copper stearate as catalysts on the performance of in-situ combustion process for heavy oil recovery and upgrading. *Journal of Petroleum Science and Engineering* **207** (12): 109125. https://doi.org/10.1016/j.petrol.2021.109125.

Yang, M. 2019. Numerical Modelling of Hybrid Steam and Combustion Recovery Process for Oil Sands (doctoral thesis). University of Calgary, Calgary, AB. https://hdl.handle.net/1880/11069.

Yang, X., and Gates, I. D. 2009. Combustion Kinetics of Athabasca Bitumen from 1D Combustion Tube Experiments. *Natural Resources Research* **18**:193-211. https://doi.org/10.1007/s11053-009-9095-z.

Yi, S., Babadagli, T., and Li, H.A. 2018. Use of nickel nanoparticles for promoting aquathermolysis reaction during cyclic steam stimulation. *SPE J*. **23** (01): 145–156. SPE-186102-PA. https://doi.org/10.2118/186102-PA.

Yuan, C., Varfolomeev, M.A., Emelianov, D.A., Eskin, A.A., Nagrimanov, R.N., Kok, M.V., Afanasiev, I.S., Fedorchenko, G.D., Kopylova, E.V. 2018. Oxidation behavior of light crude oil and its SARA fractions characterized by TG and DSC techniques: differences and connections. *Energy Fuels*. **32**(1): 801–808. https://doi.org/10.1021/acs.energyfuels.7b02377.